ACOUSTIC SCATTERING EXPERIMENTS ON SPHERES FOR STUDYING HELICOPTER NOISE SCATTERING

Jianping Yin*, Karl-Stéphane Rossignol*, Jean Bulté+
*Institute of Aerodynamics and Flow Technology, jianping.yin@dlr.de
German Aerospace Center (DLR)
Lilienthalplatz 7, 38108 Braunschweig, Germany
+ONERA (French Aerospace Center), jean.bulte@onera.fr
29 avenue de la Division Leclerc, 92320 Châtillon, France

ABSTRACT

This paper addresses first wind tunnel activities conducted in the GARTEUR Action Group HC/AG-24 dealing with acoustic scattering of spheres. GARTEUR Action Group HC/AG-24 is established to address noise scattering of helicopter rotors in presence of the fuselage. This test is a necessary step to help establishing an appropriate test setup for acoustic scattering of a generic GARTEUR helicopter model. The tests are conducted in the DLR Acoustic Wind Tunnel in Braunschweig (AWB). Two source systems, including both DLR Laser generated sound and ONERA SPARC (Source imPulsionnelle AeRoaCoustique), are used to perform shielding experiments. The tests include three spheres, two support systems and three wind speeds of 0m/s, 30m/s and 45m/s. The sizes of the spheres, a small one with 12cm in diameter and a big one with 34cm in diameter, are derived according to the maximum dimension of the BO105 fuselage with 12.5 scales down in both lateral- and stream-wise directions to consider that the scaled rotor noise frequencies fit inside the effective frequency band of the noise sources. In the current paper, the analysis of the data post-processing steps required for obtaining correct spectral and time domain data for laser sound source is emphasized. The influence of the support systems on the acoustic scattering field is analyzed. The comparison of the test results with analytical solution of sphere sound scattering is used to verify the accuracy of the tests. In addition, the test results can also be used as database to validate numerical tools.

ABBREVIATIONS

a_∞	Speed of sound in undisturbed medium
D	Diameter of the sphere
f	Frequency
γ	Heat capacity ratio
λ	Wave length
k	Wave numbers, $2\pi/\lambda$
M_0	Mach number $M_0 = U_0 / a_\infty$
p_{tot}	Total acoustic pressure perturbation
p_i	Incident acoustic pressure perturbation
p_s	Scattered acoustic pressure perturbation
γ_T	Shielding factor $\gamma_T = p_{tot}/p_i$ or $\langle p_{tot}\rangle / \langle p_i\rangle$ for numerical or test results, respectively
r	Observer position
r_0	Magnitude of the vector from source to observer
r_s	Source position
R	Radius of the sphere
τ	Emission time
$\partial T_p / \partial \tau$	Temporal heat input
U_0	Flow speed
ψ	Azimuth angle
θ	Polar angle
AC	Action Group
AWB	Acoustic Wind tunnel in Braunschweig
GARTEUR	Group for Aeronautic Research and Technology in Europe
HC	Helicopter

SPARC	Source-imPulsionnelle AeRoaCoustique
$\langle\cdot\rangle$	Ensemble average operator

1. INTRODUCTION

A negative undesirable by-product of the helicopter during its operation is noise generation. Both the main and the tail rotors (including Fenestron) of a helicopter are major sources of noise and contribute significantly to its ground noise footprint. The main research effort in the past was concentrated on the helicopter rotor noise generation and the reduction of the noise. Even though the scattering of noise generated by helicopter rotors has been recognized as a significant influence on the noise spectra and directivity, the research effort towards the scattering of noise by the helicopter fuselage, tail boom as well as stabilizer etc. has not been extensive. Therefore, the GARTEUR Action Group HC/AG-24[1] is established to address noise scattering in presence of the fuselage. The objectives of this AG are (1) to develop and validate numerical prediction methods and (2) to generate a unique noise scattering database through wind tunnel test using generic configurations, such as spheres and a GARTEUR helicopter model. This paper will focus on the results from the wind tunnel activities dealing with acoustic scattering of the spheres. One purpose of choosing spheres in the test is to verify the accuracy of the complete test system, such as support systems and noise sources, microphones as well as the reliability of the test results, by comparing with available analytic solutions for this configuration. In addition, the test results can also be used as database to validate numerical tools. The numerical activities carried out in this AG are described in a separate paper presented during the forum [16]. This test is a necessary step to help establishing an appropriate test setup for acoustic scattering of the generic GARTEUR helicopter.

This paper is organized as following: the experimental setup; including wind tunnel model, noise source characteristics and acoustic instrumentation are first presented; and some samples of a small number of representative results using laser source are introduced, including; (1) the scattering results as function of frequency, (2) the influence of support systems, (3) the influence of the wind. In addition the analysis by comparing with analytic or numeric results is also presented to clarify the accuracy of the test system.

2. DESCRIPTION OF TEST SETUP

Figure 1 shows the complete test setup, including either laser source (B,C) or SPARC (Source imPulsionnelle AeRoaCoustique, E), sphere (D) and microphone (A). The detail description of the setup is given in following sections.

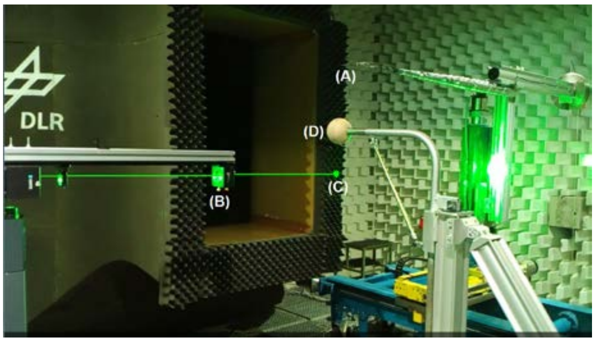

(a) Test set up with laser

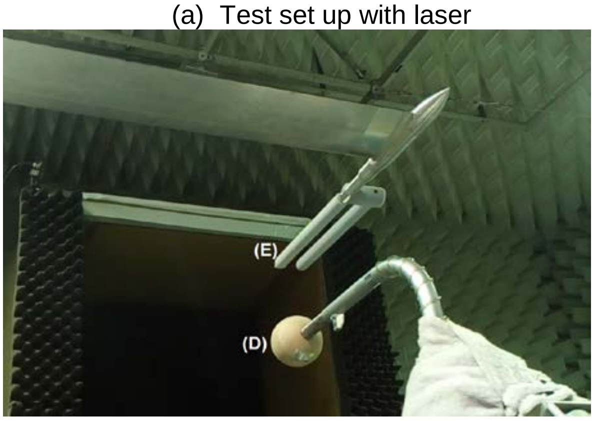

(b) Test setup with SPARC

Figure 1 Complete test set up including either laser source (B,C) (a) or SPARC (E) (b), sphere (D) and microphone (A)

2.1 Wind tunnel Facility

Simple shielding experiments on spheres are performed in the DLR Acoustic Wind tunnel in Braunschweig (AWB), as shown in Figure 1. The AWB has a cross section $1.2 \times 0.8\ m^2$. The open jet test section is known for its excellent flow quality and anechoic properties as well as its low background noise. The AWB is an open-jet wind tunnel capable of running at speeds of up to U=65m/s and is optimized for noise measurements at frequencies above 250 Hz. In current test program, the highest wind speed U=45m/s is used.

2.2 Scattering bodies and support system

2.2.1 Size of spheres

Two sphere sizes, a small one with D1=0.12m diameter and a big one with D2=0.34m diameter are used. The sizes of the spheres are derived according to the maximum dimension of the BO105 fuselage with 12.5 scales down in both lateral- and stream-wise directions, as shown in Figure 2b. Here the scale factor of 12.5 is chosen to consider that the scaled rotor noise frequencies fit inside the effective frequency band of the noise sources, so that in the test frequency range the high signal to noise ratio can be assured.

For the smaller sized sphere D1, a wooden (beech) and an aluminum sphere were tested to determine the influence of the different material impedance. For both sizes of the sphere, tests with mean flow effect are also performed.

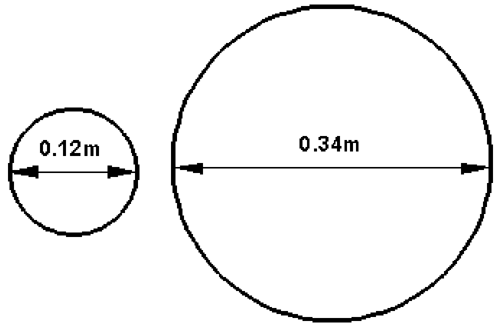

(a) Two sphere used in test

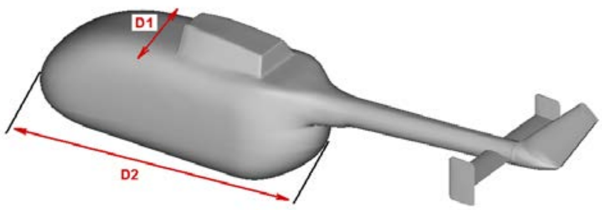

(b) BO105 model used to define sphere size

Figure 2 (a): Sphere in two different size of radius (D1=12cm and D2=34cm) used in the test; (b): Corresponding maximum dimension derived from BO105 fuselage

2.2.2 Support type in test

The system to support sphere in the test can affect scattering results. In order to check the influence of the support system on the acoustic scattering field, two support systems, sting and wires, are used in the test, as shown in Figure 3. The sting support is required for the test with mean flow. A common sting support (Figure 3 (a)) with L form is constructed for both small and large sphere. The sting is mounted in the direction parallel to tunnel central line or mean flow. The diameter and the length of the sting in flow direction are 0.028m and 0.385m respectively. To quantify the influence of the sting support on the scattering results, the wire support (Figure 3(b)) where the sphere is hanged with three 0.002m diameter wires is also used. But for the wired support, the test is conducted only without wind for safety reasons.

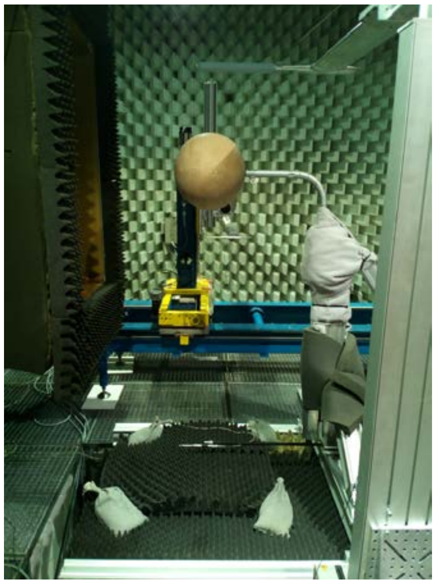

(a) Sphere with sting support

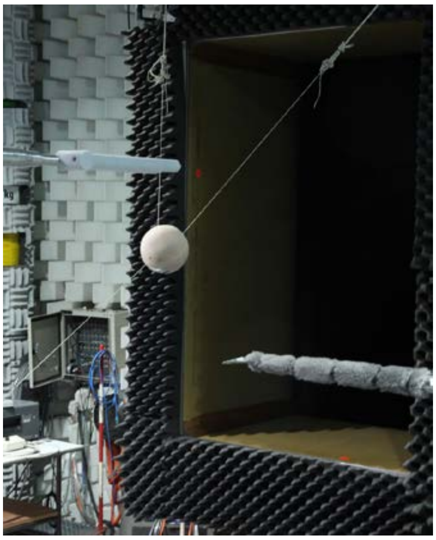

(b) Sphere with wires

Figure 3 Sphere with different support system used in the test. (a): sphere supported by sting in the test, (b): sphere hanged by wires

2.3 Description of noise sources

The choice of the noise source is based on the criterial that the noise source should have non- or minimum-intrusive for both mean flow and scattered acoustic field. As shown in Figure 1, two point source systems, the one generated from laser plasma pulse (C) and the one from

ONERA SPARC (E) are used to perform shielding experiments. Since two sources have two different frequency ranges, they compensate with each other for providing wide frequency range.

2.3.1 DLR Laser Generated Sound

By focusing a high energy laser beam to a point, it is possible to initiate the formation of a small plasma which rapidly expands [7][8], thus forming a pressure wave about its boundary which propagates through the surrounding medium. The wave equation for the pressure perturbation p' in a stagnant medium of variable mean density emphasizes the importance of the temporal heat input $\partial T_p / \partial \tau$ in generating a high amplitude pressure wave [2][3]:

(1) $$p'(\vec{r},t) = \frac{(\gamma - 1)}{4\pi a_\infty^2 r_0(\tau)} \frac{\partial T_p}{\partial \tau}$$

where γ and a_∞ is heat capacity ratio and the speed of sound in undisturbed medium, respectively. The distance $r_0(\tau)$ is the magnitude of the vector from source at emission time τ to the observer $\vec{r}$. Moreover such a pressure wave does not exhibit any directionality and decreases linearly away from its origin. The sound source is well-suited for the realization of scattering experiment at model configurations in quiescent [4][2][6] and moving mediums [3].

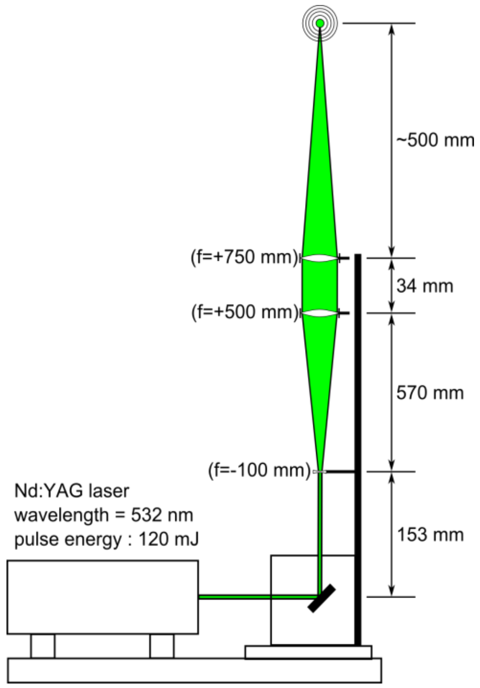

Figure 4 Optical setup for the laser sound source

A minimum amount of energy is to be provided into the medium to reach the energy threshold for the initiation of plasma formation. Once the threshold is reached, the plasma starts building up and its temperature and density increases greatly while absorbing a large portion of the input laser beam energy [9][10]. A theoretical description of the process is provided by the multiphoton ionization and cascaded ionization mechanisms [11]. In its early stage, the expanding plasma generates a pear-shaped pressure front with initial supersonic propagation speed which becomes an almost omni-directional pressure wave in the far-field [11][12]. The initial shock wave slows down to the isentropic speed of sound after approximately $20\mu s$ at which point it propagates as an isentropic acoustic wave. Consequently the small plasma generated can be seen as a breathing sphere with 10 mm radius [4]. The value of the threshold is of about $3.5 \times 10^{12} W / cm^2$ for an irradiation of wavelength $\lambda = 532 nm$ in air and at standard atmospheric pressure [13]. The optical setup for the laser sound source is shown in Figure 4.

The DLR laser sound source has the advantage of being non-intrusive for both mean flow and scattered acoustic field. Because of its small size and uniform directivity, it can be represented as a point monopole source [2]. The frequency spectrum in Figure 5 demonstrates that the peak radiation frequency is located at about 30 kHz and the useful frequency range extends from 3 kHz to 100 kHz.

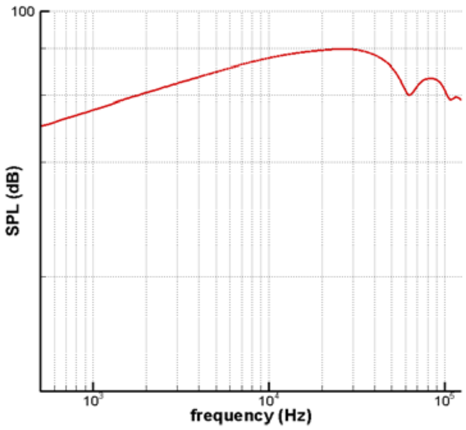

Figure 5 Typical spectrum from DLR laser pulse source (in dB)

2.3.2 ONERA SPARC (Source imPulsionnelle AeRoaCoustique)

Above a given threshold, a strong electric field ionizes the air between two sharp probes [18]. In this way, an electrical channel is created and an abrupt current dis-charge occurs. A part of the released energy is then converted into heat in the small region between probes. This intense heat induces a local expansion of the air which generates an acoustic pressure wave. A detailed setup of the sharp probes is shown in Figure 6.

Figure 6 A detailed setup of the sharp probes from SPARC

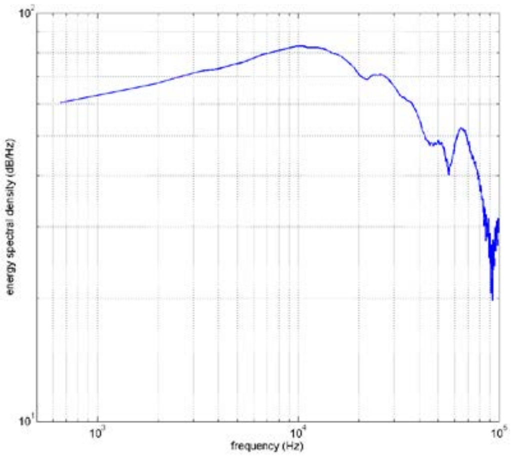

Figure 7 Typical spectrum from ONERA spark pulse source (in dB/Hz)

The maximum peak frequency for ONERA SPARC is located at about 10 KHz with useful frequency range starting from 1 KHZ, Figure 7. Therefore, the two noise sources cover different frequency ranges.

2.4 Acoustic instrumentation

In-flow measurements are performed using 1/8" inch Bruel & Kjäer pressure field microphones equipped with a standard nose cone. One microphone is installed at a fixed position near the ground and serves as a reference measurement. The second microphone is mounted on a traversing system, which is either above or below the sphere depending position of the source, as shown in Figure 1 and Figure 8 in zoom.

Figure 8: 1/8" inch Bruel & Kjäer microphone on traversing arm

When a shielding object is present between the sound source and a remote receiver, one has to be more careful; in order to make sure that only the meaningful part of the measured signal is kept for further processing and the reflections from other objects (such as wind tunnel ground, nozzle, etc.) are excluded from the signal. The test from previous campaign [2][3] indicates acoustic treatment of the ground, nozzle and positioning elements was not necessary, as reflections generally don't play an important role when using the laser or SPARC sound source, due to the very short duration of the generated pressure pulses (less than 0.1 ms for laser as example).

Because in-flow measurements are made, it is necessary to use a nose cone in front of the microphone sensing membrane. The main effect of the nose cone on the measurements is to force a shift of the spectral maximum to higher frequencies (in Figure 9, from $\approx 30kHz$ to $\approx 50kHz$), while amplifying the high-frequency spectral levels. Therefore, a supplementary and necessary correction is required to recover correct source powers and time signatures when measuring in-flow [4][2].

However, the general assumption in [2] that the nose cone correction is mostly dependent on the nose cone geometry appears, based on the current experience with the source, not to be completely true. A derivation of the correction curves is necessary for each particular test case considered and is difficult to obtain and to generalize for the highest frequencies. In Figure 9, the source spectra for three different microphone positions at $M_0 = 0$ $M_0 = 0$ are plotted. The data are not corrected in any matter. Each group of lines contains three curves, one for a microphone position upstream of the source ($\theta_i > 90°$), one for a microphone directly below the source ($\theta_i = 90°$) and one downstream of the source ($\theta_i < 90°$). A striking observation is that the nose cone effectively removes any significant θ_i dependency on the measurements in the range of measurements relevant for the present experiment (see Figure 9). This statement also holds when $M_0 > 0$, although with a slightly larger spreading (less than $\pm 1dB$), of the microphone output over the same range of measurements.

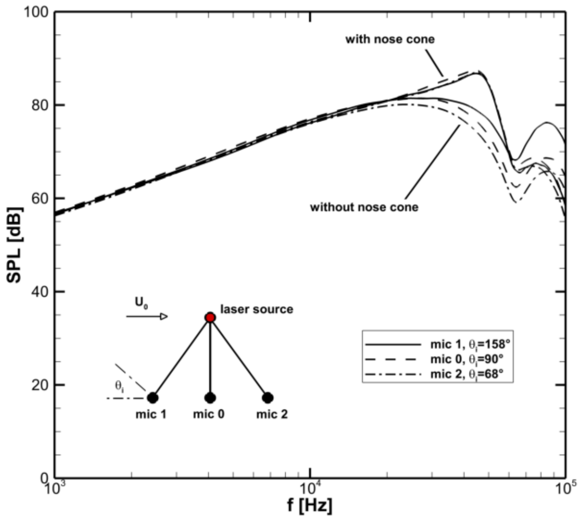

Figure 9: Effect of the nose cone on measured noise spectra ($M_0 = 0$)

In effect, the in-flow microphone gives the same output independently of its position relative to the source. As the source is known to radiate uniformly with monopole character [4][5][7] the assumption is absolutely correct. This independence vs. θ_i of the measured data simplifies greatly the calculation of accurate shielding coefficients as the application of correction procedures can be omitted. This is particularly interesting in cases where a precise propagation direction of the radiated sound field, and therefore of its incidence on the microphone, cannot be determined precisely or at all. All the noise shielding results presented later on were not corrected prior to the computation of the shielding factors.

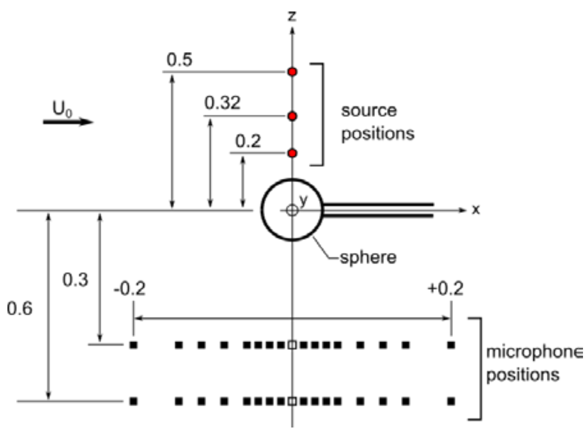

Figure 10: Source and microphone positions. Same microphone traverse for the y direction

The measurements were done on linear microphone traverses in both x (where the sting is located in this axis) and y directions and the positions of sources and microphone traverse in x direction are shown in Figure 10. As the spheres are located directly between the source and microphone, the maximum sound shielding can be measured by the arrays. Two microphone traverses are necessary in order to test the influence of the support system, such as the sting. The definition of the coordinate center is chosen as center of the sphere.

3. WIND TUNNEL TEST

The tests conducted include: Two sources (Laser and SPARC), three source positions (0.2m,0.32m,0.5m) and two array positions (0.3m and 0.6m), as shown in Figure 10, three spheres (D=0.12m in aluminum and wood, D=0.34m in wood) and two support systems (Figure 3) as well as three wind speeds of 0m/s, 30m/s and 45m/s.

3.1 Data Acquisition and Processing

3.1.1 Data using Laser source

For the present experiment a laser repetition rate of 10 Hz and an acquisition time of 20 s were chosen. This means that approximately 200 pulses are recorded per data point.

Sound measurements, for each configuration, are performed with a continuously running laser operated at full power, in order to get the maximal possible signal to noise ratio (SNR). The laser output trigger signal is simultaneously recorded to facilitate data post-processing. For each configuration all pulses are extracted from the measured time series by correlating a reference pulse signal with the raw measurements. In cases where $U_0 > 0$ m/s, the time signals have to be band-filtered between 3 kHz and 110 kHz at $U_0 = 30$ m/s and between 5 kHz and 110 kHz at $U_0 = 45$ m/s respectively, to remove low-frequency contamination of the data through flow-induced noise on the microphone body as well as from vibrations of the microphone support. Filtering of the raw time series is necessary for a better extraction of the pulses during post-processing, especially when investigating the shielded sound field, where the absolute amplitude of the sound pulses is greatly reduced.

Prior to the calculation of averaged time domain data, the individual extracted pulses are superposed through peak locking of the first pressure maximum. Fourier analysis, of the individual and averaged pulses, is then performed using non-overlapping blocks zero-padded to a total length of 4096 samples for a frequency resolution of $\Delta f = 61\,\mathrm{Hz}$. This block length is kept constant throughout the post-processing even when single pulses were measured. The reasons behind this choice are twofold. First, enough samples are needed to ensure the complete recovery of the meaningful part of the signals when measuring with the shielding object installed. Second, a constant and consistent block length has to be defined for a correct representation of the pulses full energy content in both the shielded and free-field cases and a necessity for the recovery of correct shielding factors. Finally, no window function is applied to the signals prior to FFT computations as the pulses are short-time signals which tend to zero quickly towards the block's bounds.

Since dealing with a pulse of very short duration (≈ 0.1ms), very high sampling rates are needed. The available acquisition unit (GMB Viper,48 channels) was therefore used at its maximal acquisition rate of 250 kHz with an anti-aliasing filter cut-off frequency fixed at 100 kHz. This setup enables a correct sampling of signals with frequencies up to approximately 100 kHz. Although, in cases where $U_0 > 0$ m/s, an upper frequency of 80 kHz is considered in the analysis due to a poor SNR for frequencies above this limit. In order to measure at such frequencies, 1/8" G.R.A.S. 40DP microphones with a 140 kHz dynamic range were used.

4. ANALYTIC SOLUTION OF ACOUSTIC SCATTERING FROM RIGID SPHERE

There are analytic solutions of the acoustic scattering of a point monopole source from a 3D hard sphere in a medium in rest. The solution can be derived from the Helmholtz Equation using Green's function, solid wall and far field bound condition. The formulation described in following section can also be found in [14][15][16].

4.1 Formulation for analytic solution

Consider the acoustic scattering of a point monopole source by a rigid sphere of radius R, with microphones located at the spherical coordinates (r,θ,ϕ) and a source located at a distance r_s positioned on the z axis at $\theta = 0°, \phi = 0°$ as shown in Figure 11).

The analytical solution of the total pressure is given in equation 2:

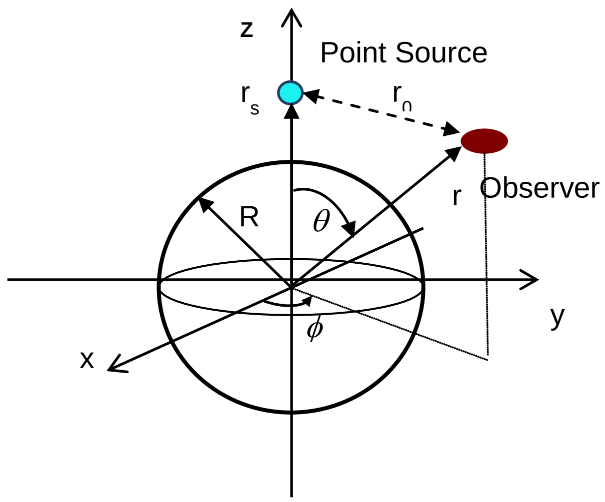

Figure 11 Scheme of acoustic scattering of a point monopole source by a sphere

(2a)

$$p_{tot}(r,\theta)=\frac{i\,k}{4\pi}\sum_{m=0}^{\infty}\{(2m+1)[j_m(kr)\,h_m^{(1)}(kr_s)-\frac{j_m{}'(kR)}{h_m^{(1)}{}'(kR)}h_m^{(1)}(kr_s)h_m^{(1)}(kr)]P_m(\cos\theta)\},\quad r\le r_s$$

(2b)

$$p_{tot}(r,\theta)=\frac{i\,k}{4\pi}\sum_{m=0}^{\infty}\{(2m+1)[j_m(kr_s)\,h_m^{(1)}(kr)-\frac{j_m{}'(kR)}{h_m^{(1)}{}'(kR)}h_m^{(1)}(kr_s)h_m^{(1)}(kr)]P_m(\cos\theta)\},\quad r> r_s$$

where $k=2\pi/\lambda$ is wave number and $P_m(z)$ is the zeroth degree Legendre function of first kind of order m, $j_m(z)$ and $h_m^{(1)}(z)$ are the spherical Bessel and Hankel functions of the first kind and order m, whereas $j_m{}'(z)$ and $h_m^{(1)}{}'(z)$ denote the derivative terms computed as:

$$j_m{}'(z)=-j_{m+1}(z)+\frac{m}{z}j_m(z)$$

$$h_m^{(1)}{}'(z)=-h_{m+1}^{(1)}(z)+\frac{m}{z}h_m^{(1)}(z)$$

The spherical Bessel and Hankel functions are related to the Bessel and Hankel functions by the following identities:

$$j_m(z)=\sqrt{\frac{\pi}{2z}}\,J_{m+1/2}(z)\,,\quad h_m^{(1)}(z)=\sqrt{\frac{\pi}{2z}}\,H_{m+1/2}^{(1)}(z)$$

Detail description on numerical activities within this GARTEUR AG 24 is given in [16].

Figure 12 shows the contour plot of the total pressure p_{tot} (Equation 2) on a receiving plane (microphones) located at $Z_m=-0.30$ m for three different frequencies, 3000Hz, 7500Hz and 15000Hz, which are used in the following section for evaluating test results. For the analytic solutions, a point source is located at $Z_s=0.32$ m on the z axis and the size of for sphere chosen for this example is D=0.12m. Two dashed lines represent two traverse directions during measurements. The Points Per Wave length (PPW) used in the simulation are 28 for 3000Hz and 7500Hz and 22 for 15000Hz, respectively. This number will be used to discretize the sphere in all following simulations, unless it is redefined.

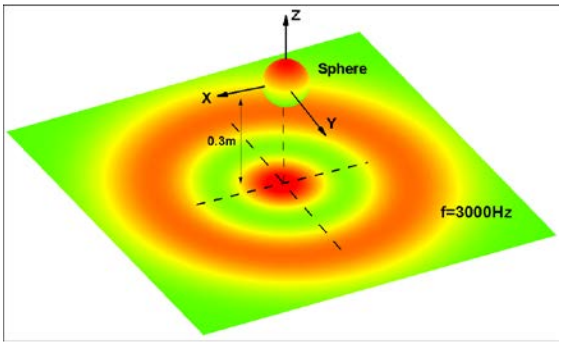

(a) f=3000Hz, $kD=6.65$

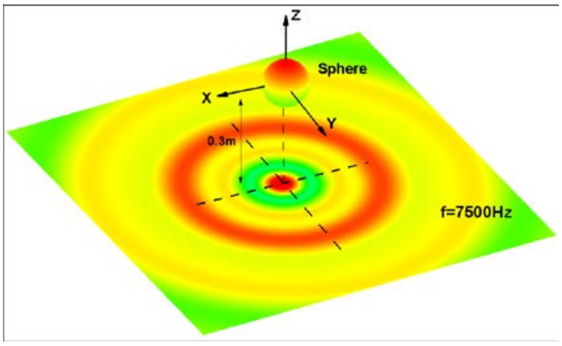

(b) f=7500Hz, $kD=16.63$

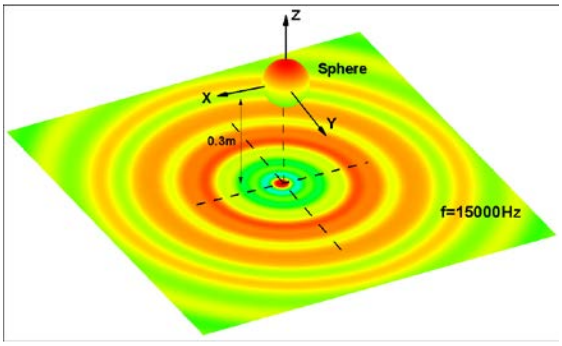

(c) f=15000Hz, $kD=33.26$

Figure 12 contour plot of the total pressure p_{tot} for D=0.12m, $Z_s=0.32$ m and various kD

The general shielding characteristics can be observed by the shielding pattern with symmetric bands of higher and lower shielding levels in the plot. The higher and lower levels are represented by different colors in Figure 12. The "silent zone" direct below the sphere, where no incident wave can be propagated there directly, are determined entirely by the diffracted waves, which has a small peak showing in red area for the given $kD = (2\pi / \lambda)D$. The area of the peak is then decrease with increasing kD. In addition, with increasing kD, the number of bands of higher and lower shielding levels is increased, indicating the increases the complexity in wave interference in high frequency. In general, the complexity of the scattering pattern increases with increasing kD. These shielding characteristics are more visible in Figure 13, when comparing the values taken directly from the microphone traverse marked as dashed line in x and y direction. As limited microphone traverse positions in the measurement were measured, the comparison with experiment in the following sections is limited to the area marked as vertical dashed line in Figure 13.

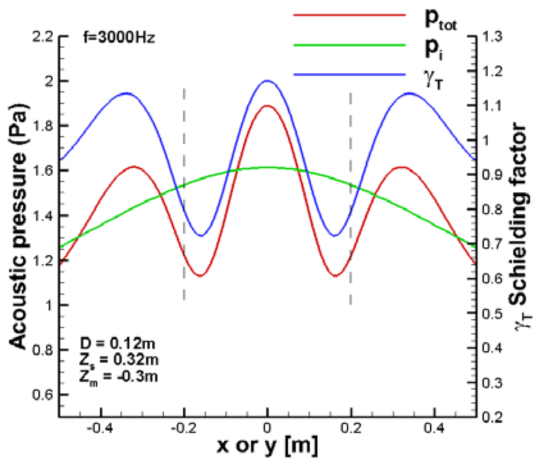

(a) f=3000Hz, $kD = 6.65$

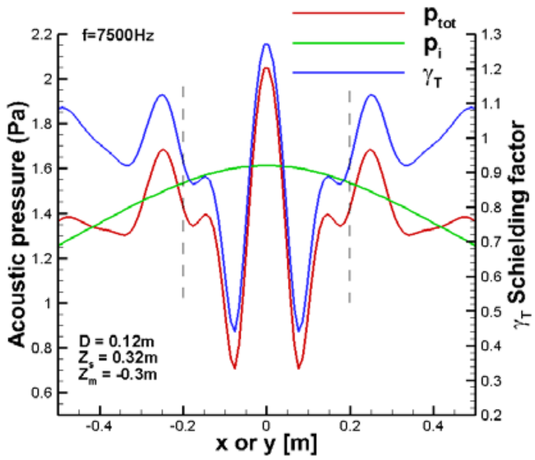

(b) f=7500Hz, $kD = 16.63$

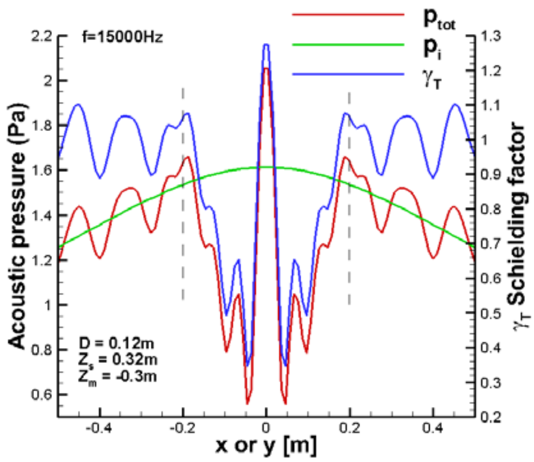

(c) f=15000Hz, $kD = 33.26$

Figure 13 the total p_{tot} and incident p_i acoustic pressure as well as shielding factor $\gamma_T(f) = p_{tot}(f) / p_i(f)$ for a sphere (D=0.12m) scattering

When comparing with incident pressure p_i (green line) in Figure 13, the total pressure p_{tot} (red line) under influence of the sphere has created local peak value underneath the sphere (x or y=0) which is greater than p_i for all three frequencies given here. The peak area decreases with increasing the frequencies. The smooth curved surfaces of the sphere lead to smooth transition of the total pressure from one region to another. As explained before, the complexity of the interference increases with increasing kD and is in general dependent on the source location in relation to the diffraction edges (sphere surface), as well as the source directivity, the source coherence (diffraction from different part of the surfaces) and kD.

5. TEST RESULTS AND DISCUSSION

In following sections, only the comparison of the shielding factor for the test and analytic or numerical results is conducted. The shielding factor is defined as the ratio of total pressure, P_{tot} and incident pressure p_i,

$$\gamma_T(f) = \frac{\langle p_{tot}(f)\rangle}{\langle p_i(f)\rangle}$$

Where $\langle p_{tot}(f) = p_s(f) + p_i(f)\rangle$ and $\langle\bullet\rangle$ are the ensemble averaged total and incident pressure fluctuations. The $p_s(f)$ is scattered pressure fluctuation which can only be obtained from simulations. Therefore the shielding factor deviation from 1 can be considered as the effect of the scattering from any obstacle.

In case of evaluating shielding factor for analytical or numerical simulation, the shielding factor is direct evaluated from $\gamma_T(f) = p_{tot}(f) / p_i(f)$ and no ensemble averaging is required.

The advantage of using shielding factor to evaluate the scattering effect is that no corrections on signal amplitude are required. In addition, when the microphone equipped with nose cone during the measurement, the corrections on microphone directivity are not required as the nose cone effectively removes any significant dependency on the measurements in the range of measurements relevant for the present experiment.

In this section, the test results are also compared with the calculations obtained with the analytical formulation (2a or 2b), to verify the accuracy of the complete test system, such as support systems and noise source, microphones as well as the reliability of the test results.

The following sphere scattering results will be presented:

1. Comparison of the measured shielding factor with analytic results at selected frequencies;

2. Comparison of the influence of the support systems at selected frequencies;

3. Scattering under the influence of different wind speeds.

5.1 Case1: $U_0 = 0$ m/s, $D = 0.12$ m and $D = 0.34$ m, Source at $Z_s = 0.32$ m, microphone traverse $Z_s = -0.30$ m

The arrangement of the source, microphone positions and the sphere for case 1 is given in Figure 14.

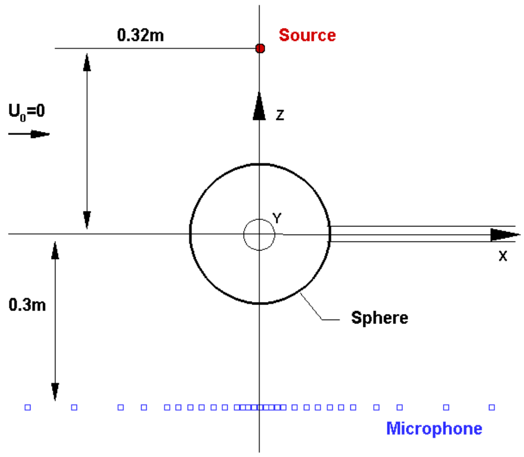

Figure 14 Source and microphone positions for case 1

5.1.1 At f=3000Hz with laser source

The acoustic signal at 3000Hz has a wave length at about $\lambda = 0.113$ m, which is close to the characteristic length of the small sphere diameter D=0.12m. Therefore a strong interference in space is expected for this frequency. The tests have been conducted using two different support systems, sting and wire as shown in Figure 3 to verify if the effect of the sting can be identified.

As shown in Figure 15, the measured shield factors for the sphere hanged with wires (D=0.002m, Figure 3b) fit the best with analytic (blue line) in both array directions. Both the analytic solution (blue line) and measured results indicate the troughs and peaks of an interference pattern around the shadow region where the microphones are located below sphere around (x,y) = (0,0). The interference of the diffracted wave from the sphere has caused a resultant wave with a greater amplitude than incident wave (γ_T>1) underneath the sphere. It has to be mentioned that there is slightly offset in the microphone coordinates in the test (within 0.01m) in x or y direction, which has been corrected in Figure

15. As expected, the scattering of the wires is negligible in this frequency.

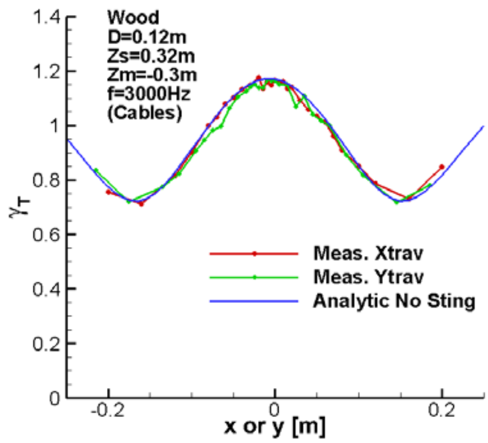

Figure 15 Measured shielding factor γ_T for the wood sphere D=0.12m with cable support at 3000Hz (offset in microphone coordinate corrected)

As no analytical results with respect to the configuration with the sting support can be used for comparison, the numerical simulation using DLR fast multiple boundary element method (FMBEM) [16][17] is conducted in order to demonstrate the influence of the sting. Figure 16 shows the numerical simulation of the contour plot for the total pressure p_{tot} on a receiving plane (microphones) located at $Z_m = -0.30$ m. Due to the contribution of the diffraction waves from the sting support the shielding pattern is no more symmetric in comparing with Figure 12 (a), especially for the area underneath the sting support.

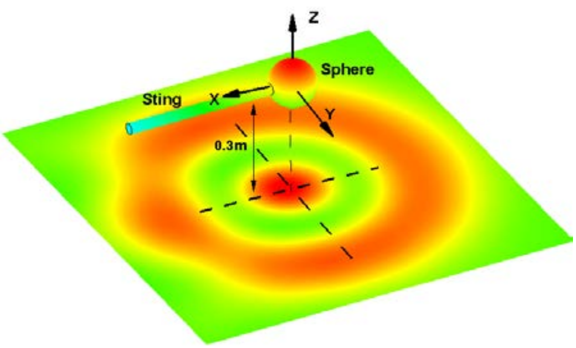

Figure 16 the contour plot of the total pressure p_{tot} for D=0.12m, $Z_s = 0.32$ m and f=3000Hz, influence of the sting included

Figure 17(a) and (b) show the comparisons of measured shielding factor γ_T for both the aluminum and the wood sphere with analytical one (solid blue line). In comparison with the analytical one (without the sting), the general characteristics of the local peak and valley from the scattering of the sphere are captured for both spheres. The deviations of the test results from the analytical one in the positive x directions indicate the interference from sting support. The shielding factor γ_T for the microphones on Xtrav underneath the sting support (in red line) is larger than that for the Ytrav microphones, which indicate the enhancement of the sound field from the sting. As expected, with increasing the distance from the sting, for example in positive x or y direction, the influence of the sting decays. The test results from Ytrav indicate symmetric pattern along y direction for both aluminum and wood sphere. The test results from both aluminum and wood sphere display similar behavior, except the test results from the aluminum sphere showing a clear offset in amplitude from analytic solution in comparing with wood sphere. This systematic offset also occurs for the other frequencies given in following sections. The reasons may devote to the possible deviation of the source position relative to sphere or microphone, changing source strength in the measurement with and without sphere, microphone position relative to source or sphere, etc., but this offset still need to be clarified.

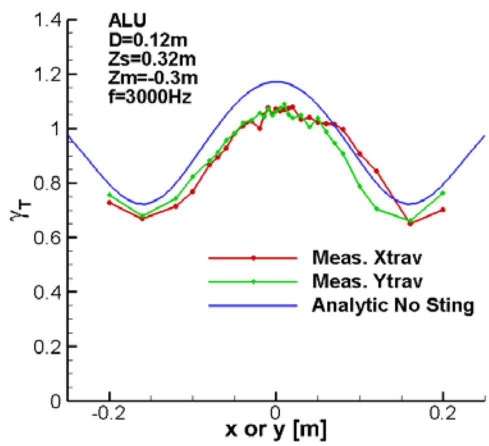

(a) aluminum sphere

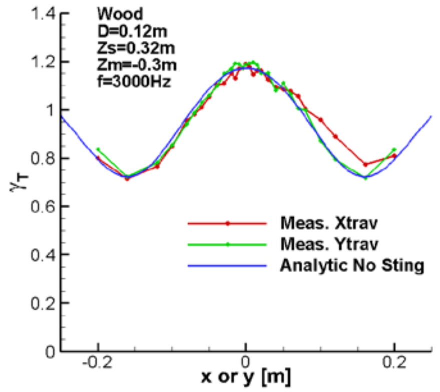

(b) wood sphere

Figure 17 Shielding factor γ_T for the aluminum and the wood sphere D=0.12m with sting support at 3000Hz

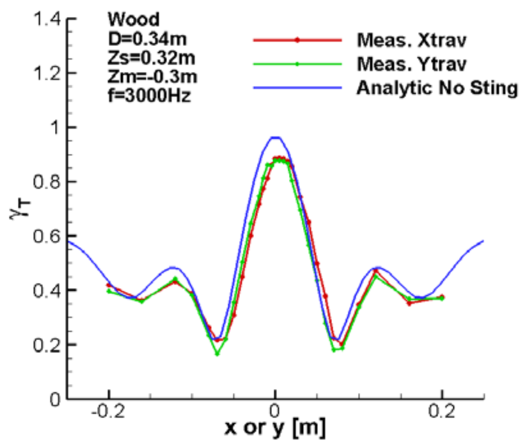

Figure 18 Shielding factor γ_T for the wood sphere D=0.34m with sting support at 3000Hz

In case of large sphere ($D = 0.34m$) scattering where $\lambda \ll D$ as shown in Figure 18, the shielding factors exhibit a narrow shadow region and lower value of the shielding factor in comparing with small sphere for this frequency. The interference of the diffracted wave has caused a resultant wave of lesser amplitude (quieter) than the incident wave p_i (γ_T<1) and form a clear two side lobes along edge of the sphere, which indicate increasing complexity in the interference of the diffracted wave and more reflection of the energy by the sphere in the direction opposite to the microphone. The measured shielding factors on two arrays almost coincide with each other, which indicate decreasing the influence of the sting on the shielding factors.

The comparisons of the shielding factor for two sizes of spheres indicate that the coherence between test and analytical results for this frequency is captured by the test. More shielding effect and less effect from sting support system interference are observed for large sphere.

5.1.2 f=7500Hz with laser source

The acoustic signal at 7500Hz has a wave length at about $\lambda = 0.0453$ m, which is now smaller than the characteristic length of the small sphere diameter D=0.12m. The interference pattern in space, as shown in Figure 19, indicates a local peak in shadow area and two side lobes in the displayed area. The width of the peak area in the shadow zone becomes narrower in comparing with 3000Hz case (Figure 17), but the amplitude of the peak increases slightly. The offset observed for aluminum sphere at 3000Hz in comparing with the results of the wood sphere (Figure 17) occurs also for this frequency. The sting effects for the small sphere (Figure 19, Figure 20) indicate a decreasing the shielding factor of the Xtrav for the microphone positions underneath the sting, which is opposite to the results from the previous section with f=3000Hz.

For the large sphere the interference patterns (Figure 21) become more complicated by showing more side lobs. The tests resemble the similar behavior as the analytic one and demonstrate the small effect from the sting. In addition, the test has captured at least the first two lobes.

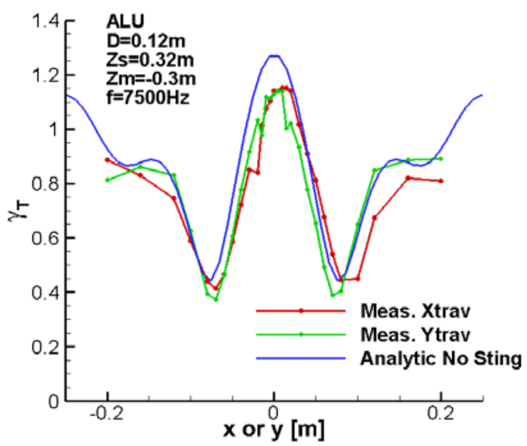

Figure 19 Shielding factor γ_T for aluminum sphere D=0.12m with sting support at 7500Hz

In general for this frequency, although there is some level of disagreement in representing the side lobs, the test results are comparable with the analytical one in acceptable accuracy.

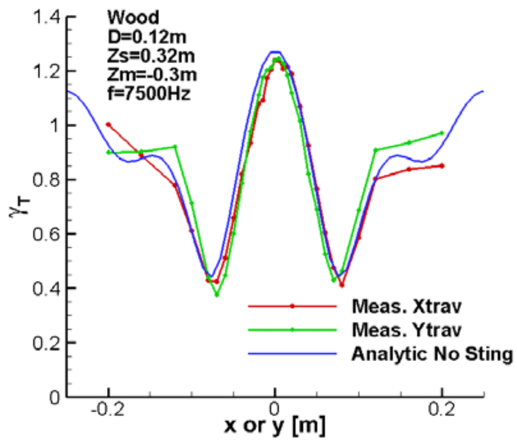

Figure 20 Shielding factor γ_T for the wood sphere D=0.12m with sting support at 7500Hz

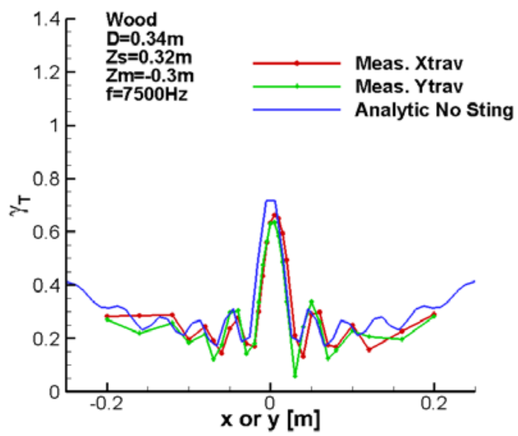

Figure 21 Shielding factor γ_T for the wood sphere D=0.34m with sting support at 7500Hz

5.1.3 f=15000Hz with laser source

The offset observed for aluminum sphere (Figure 22) is again observed in this frequency. As the acoustic signal at 15000Hz has a wave length at about $\lambda = 0.022$ m, which is close to the diameter of the sting (D=0.028m), a strong influences of sting support for the shielding factor in the small sphere (Figure 22 and Figure 23) cases are expected for microphones beneath the sting (positive x).

For the results from large sphere (Figure 24), the strong reflection of the acoustic energy from sphere causes large shadow region (γ_T <<1). For this case, there is general agreement in averaged form between the test and the analytic results, except the test shows several side lobes which are not given in the simulation.

In comparison with the results from other frequencies, the general shielding characteristics indicate that with increasing the frequency, the width of the peak area in the shadow zone becomes narrower, the side lobes become sharper and the number of side lobes becomes larger.

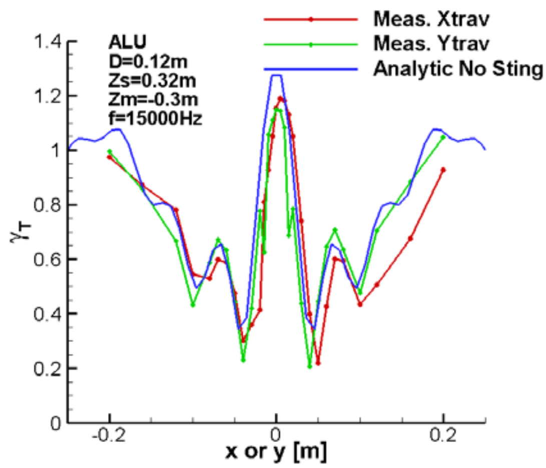

Figure 22 Shielding factor γ_T for the aluminum sphere D=0.12m with sting support at 15000Hz

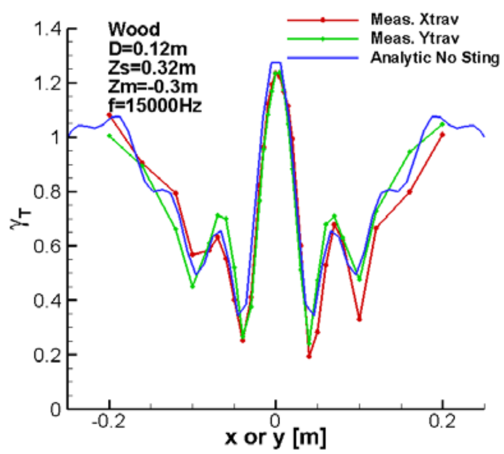

Figure 23 Shielding factor γ_T for the wood sphere D=0.12m with sting support at 15000Hz

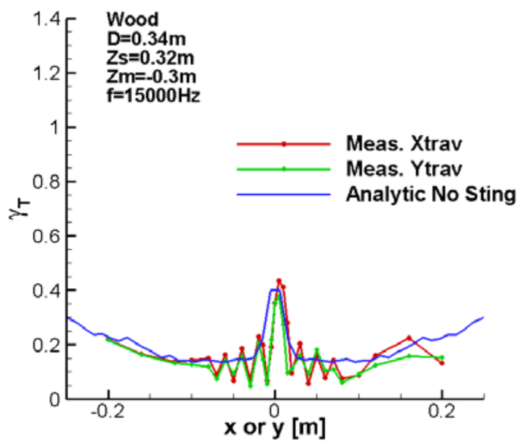

Figure 24 Shielding factor γ_T for the wood sphere D=0.34m with sting support at 15000Hz

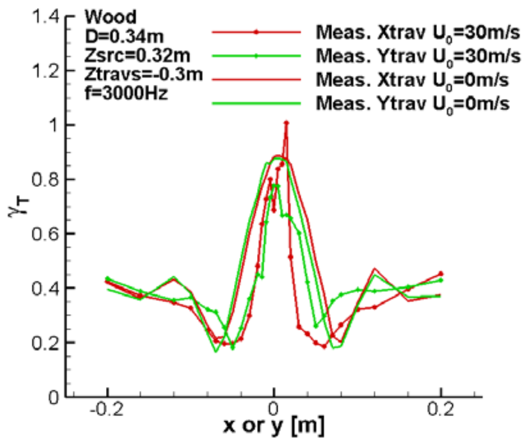

Figure 25 Shielding factor γ_T for the wood sphere D=0.34m with sting support at 3000Hz

5.2 Case2: $U_0 = 30.0$ m/s, $D = 0.34$ m, Source at $Z_s = 0.32$ m, microphone location $Z_s = -0.30$ m

A schematic representation of the experimental system is given in Figure 14.

Both Figure 25 and Figure 26 show the comparison of shield factor in the condition with and without mean flow in two frequencies. In the case with mean flow, the width of the main peak area (red or green line with solid symbols) in the shadow zone (around x or y =0) becomes narrower which is similar to the phenomenon by increasing the frequency observed in the previous sections in the case without mean flow. Therefore, this phenomenon may be corresponding to the Doppler Effect caused by the mean flow speed. Another effect of the presence of the mean flow is to refract the scattered sound so as to shift the location of the lobes. The effect of mean flow has smooth up the side lobes especially for microphones in the direction of the flow (x-direction).

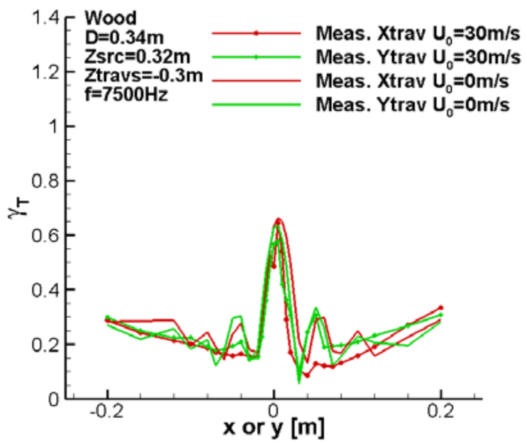

Figure 26 Shielding factor γ_T for the wood sphere D=0.34m with sting support at 7500Hz

6. CONCLUDING REMARKS

In this paper, experimental investigations of the shielding characteristics of spheres and comparison with analytical solution are presented. One purpose of the test is to verify the accuracy of the complete test system, such as two support systems and two noise sources, microphones as well as the reliability of the test results. Following concluding remarks can be drawn as following:

The laser-based non-intrusive sound source utilized in this study allows a direct measurement of the shielding factors both in quiescent and moving mediums. The noise shielding results provide clear and consistent trends for all cases considered. The dependency of the shielding factor on frequency or sizes of the sphere or support system are captured. For the present shielding configuration, the test setup with laser source provides an acceptable level of accuracy in the test. But the offset in shielding factor for aluminum sphere and oscillations of the side lobes in measurement results for large sphere at 15000Hz are still need to be clarified.

The influence of the sting on the shielding factors of the sphere cannot be ignored for the small sphere. Therefore when using the test data for the purpose of the code validation, the sting influence needs to be considered in the numerical simulation. The wire support provides least influence of the wires on the measurement data.

With respect to the microphone corrections, as the nose cone effectively removes any significant dependency on the measurements in the range of measurements relevant for the present experiment, therefore no corrections on microphone are required in determining the shielding factor. When the focus is on recovering correct absolute quantities from measurements, the aspect of microphone corrections is found to be of critical importance both in the time and frequency domains, and for frequencies above 10 kHz.

In this paper, the test results and their comparisons with the analytical solutions provide a high confidence on establishing an appropriate test setup for acoustic scattering problems. The next step is to apply the experiment procedure to noise shielding investigations of the generic GARTEUR helicopter.

AKNOWLEDGEMENTS

The work reported is part of activities conducted in GARTEUR Action Group HC/AG-24. Special thanks go to Jurrien Olsman, Michael Pott-Pollenske for their efforts in preparation and conduction of this test.

REFERENCES

[1] J. Yin, M. Barbarino, H. Brouwer, G. Reboul, M. Gennaretti, G. Bernardini, C. Testa, L. Vigevano, “Helicopter Fuselage Scattering Effects for Exterior/Interior Noise Reduction”, Terms of Reference for the GARTEUR Action Group HC/AG-24, April 2015.

[2] K.-S. Rossignol, J. Delfs, F. Boden, “On the Relevance of Convection Effects for a Laser-Generated Sound Source”, 21th AIAA/CEAS aeroacoustics conference, AIAA 2015-3146 Dallas, USA, June 2015

[3] K.-S. Rossignol, J. Delfs. "Analysis of the Noise Shielding Characteristics of a NACA0012 2D Wing", 22nd AIAA/CEAS Aeroacoustics Conference, Lyon, France, 2016

[4] F. Boden, J. Delfs, “Development of a laser-based sound source,” Inter-Noise, Honolulu, Hawaii; USA, December 2006.

[5] F. Boden, „Grundlagenuntersuchungen zu einer neuartigen Laserschallquelle“, Tech. Rep. IB 124-2007/5, DLR, Braunschweig, Institut für Aerodynamik und Strömungstechnik, 2007.

[6] K.-S. Rossignol, M. Lummer, J. Delfs, “Validation of DLR's sound shielding prediction tool using a novel sound source”, Proceedings of the 11th AIAA/CEAS aeroacoustics conference, AIAA 2009-3329

[7] N. Hosoya, M. Nagata, I. Kajiwara, “Acoustic testing in a very small space based on a point sound source generated by laser-induced breakdown: Stabilization of plasma formation”, Journal of Sound and Vibration, Vol. 332, No. 19, 2013, pp. 4572-4583

[8] L. Radziemski, D. Cremers, “Laser induced plasmas and applications”, Marcel Dekker Inc., New-York, June 1989

[9] T. X. Phuoc C. M. White, “Experimental studies of the absorption and emissions from laser-induced spark in combustible gases”, Optics communications, Vol. 181, No. 4, 2000, pp. 353-359

[10] Y.-L. Chen, J. Lewis, C. Parigger, “Spatial and temporal profiles of pulsed laser-induced air plasma emissions”, Journal of quantitative spectroscopy and radiative transfer, Vol. 67, No. 2, 2000, pp. 91-103

[11] G. Ostrovskaya. A. Zaidel', “Laser spark in gases”, Physics-Uspekhi, Vol. 16, No. 6, 1974, pp. 834-855.

[12] M. Villagrán-Muniz, H. Sobral, R. Navarro-González, “Shock and thermal wave study of laser-induced plasmas in air by the probe beam detection technique”, Measurement Science and Technology, Vol. 14, No. 5, 2003, pp. 614.

[13] T. X. Phuoc, “Laser spark ignition: experimental determination of laser-induced breakdown thresholds of combustion gases”, Optics Communications, Vol. 175, No. 4, 2000, pp. 419-423.

[14] J. J. Bowman, T. B. A. Senior and P. L. E. Uslenghi, “Electromagnetic and acoustics scattering by simple shapes”, North Holland Publishing Company, Amsterdam, 1969.

[15] M. Barbarino, H. Brouwer, G. Reboul, L. Vigevano, J. Yin, “Collection of analytical solutions and experimental results for acoustic scattering”, GARTEUR AG24 deliverable, AG24-D1,15.05.2015

[16] M. Barbarino, D. Bianco, J. Yin, M. Lummer, G. Reboul, M. Gennaretti, G. Bernardini, C. Testa, “Acoustical methods towards accurate prediction of rotorcraft fuselage scattering”, ERF 2016

[17] M. Lummer, ,C. Richtery , C. Pröber, J. Delfs, “Validation of a Model for Open Rotor Noise Predictions and Calculation of Shielding Effects using a Fast BEM”, 19th AIAA/CEAS Aeroacoustics Conference (34th AIAA Aeroacoustics Conference), 27 - 29 May 2013.

[18] P. Lebigot, J. Bulté, R. Davy, F. Desmerger, L. Coste, "SPARC: Source imPusionnelle AéRoACoustique", ONERA Technical Report (in French), N°4/22699, 2015.

COPYRIGHT STATEMENT